JOURNAL OF APPLIED ELECTROCHEMISTRY 24 (1994) 703–712

Mathematical reactor modelling for coupled chemical and electrochemical processes: the ECE system

K. SCOTT

Department of Chemical and Process Engineering, University of Newcastle upon Tyne, Merz Court, Newcastle-upon-Tyne, NE1 7RU, Great Britain

A. N. HAINES

British Steel Technical, Swindon Laboratories, Rotherham, S60 3AR, Great Britain

Received 18 November 1993; revised 20 January 1994

A procedure for modelling electrochemical reactions and reactors which involve heterogeneous reaction, homogeneous fast chemical reaction and diffusional mass transport is described. The procedure can be applied to any combination of first order reaction processes utilising numerical routines for the solution of initial value differential equations. By the use of collocation it can be extended to higher order processes. The reactor types considered are batch, plug flow and dynamic continuous stirred tanks and reactors with recycle. Operation with either potentiostatic, galvanostatic or constant cell voltage control is described and illustrated using the ECE reaction mechanism, involving successive electrochemical, chemical and electrochemical reaction.

List of symbols

a_e	specific area of the electrode (m^{-1})
b	Tafel slope (mV)
c	concentration ($kmol\,m^{-3}$)
d	interelectrode gap (m)
D	diffusion coefficient ($m^2\,s^{-1}$)
E	electrode potential (V)
E_c	cell voltage (V)
E_e	equilibrium potential
F	Faraday's constant ($C\,mol^{-1}$)
Ha	Hatta number as in Equation 11
i	current density ($kA\,m^{-2}$)
i_L	mass transfer limiting current density ($kA\,m^{-2}$)
k_{fi}	rate constant or coefficient (heterogeneous) ($m\,s^{-1}$)
	rate constant (homogeneous) (s^{-1})
k_{Li}	mass transfer coefficient ($m\,s^{-1}$)
N	molar flux ($kmol\,m^{-2}\,s^{-1}$)
n	number of electrons transferred
Q	flowrate ($m^3\,s^{-1}$)
R	recycle ratio
r	reaction rate ($kmol\,m^{-3}\,s^{-1}$)
t	time (s)
V	volume of reactor (m^3)

Greek symbols

δ	diffusion layer thickness (m)
α	transfer coefficient
β	slope of kinetic polarization curve (V^{-1})
τ	space time (s)
η	over potential (V)
χ	electrolyte conductivity ($\Omega^{-1}\,m^{-1}$)

Superscripts

b	in the bulk solution
s	at the electrode surface
z	distance from the electrode surface within the diffusion layer

Subscripts

1, 2, 3	step number
a	anode
c	cathode
e	electrode surface or reactor exit
f	heterogeneous
i	ith reaction or reactor inlet
j	species J
T	total
r	recycle loop
0	initial value
h	solvent decomposition

1. Introduction

The limitations necessary to derive analytical solutions for electrochemical reactor systems have led to solution of the governing differential equations by numerical methods. In this way, particularly if solutions in dimensionless form are generated, the results may be more generally useful. There have been several examples of this approach to electrochemical reactor systems [1–3] which solve the governing equations for electrochemical/chemical reaction schemes by finite difference techniques.

Alkire and Mirarefi [4–6] developed a computational method to calculate current distribution

0021-891X

along the length of a tubular electrode under fully developed laminar flow conditions. Alkire and Gould [7] used numerical techniques similar to those reviewed by Feldberg to analyse the performance of multiple reaction sequence in a porous electrode through which electrolyte was passed. White and coworkers have developed models to predict behaviour at rotating disc electrodes [8] and in parallel plate cells [9, 10].

Alkire and Lisius [11, 12] developed a detailed model of propylene oxide production in a parallel plate reactor. This reaction utilizes both anodically and cathodically generated intermediates and several chemical reactions were included. These reactions occurred in the diffusion layer at the anode. Yung and Alkire [13] developed a similar model for a laminar flow reactor with gas evolution at both electrodes.

There have been several models developed for multiple reactions in packed bed or porous electrodes [14, 15]. A model for paired synthesis reactions in batch recycle reactors was applied by Yu, *et al.* [14] to the formation of 2-butanone in packed bed reactors. Oloman modelled a packed bed reactor [15] in which a two phase oxidation of benzene (as an emulsion) or benzoquinone occurred.

This present paper sets out a procedure for the simulation of coupled chemical and electrochemical reactions with diffusional mass transfer. The chemical reactions are fast and have comparable rates to that of diffusion. Using as an example the ECE reaction, the behaviour of batch, plug flow, dynamic CSTRs and recycle reactors are modelled under potentiostatic, galvanostatic and constant voltage operation. The method is applicable to many industrial systems where an excess supporting electrolyte is used and the analysis of only one electrode region is acceptable. The solution to the model is achieved using a combined analytical and numerical procedure. The latter is achieved here using a commercial software numerical simulator [16].

2. Structure of the model

Several assumptions are adopted in setting up the structure of the model of the electrochemical processes:

(i) No species accumulation in the mass transfer layer at the electrode surface.

(ii) No interaction between mass transfer coefficients in the diffusion layer.

(iii) Isochoric conditions.

(iv) Total current at the electrode is the sum of the individual currents of associated reactions.

(v) Electrochemical kinetics are described by Butler–Volmer equations and associated rate parameters are independent of time.

(vi) Chemical kinetics are first order irreversible.

(vii) There is an excess of supporting electrolyte and thus transfer or ionic reactants by migration is negligible.

The elements which make up the model overall can be summarized as:

- A model of the reaction chemistry and electrochemistry. If a simulation is performed then appropriate kinetic data is assumed in existence. For data analysis certain kinetic coefficients become adjustable parameters.
- Local conservation equations in the diffusion layer for each species. For the assumed film model, with an excess of supporting electrolyte, this is an equation based on Fick's second law of diffusion with reaction. The model can accommodate a variable diffusion layer thickness along the electrode which may arise due to hydrodynamic entrance effects or gas evolution effects within the reactor.
- Combination of the above to form an overall model of the reaction rates at one position on the electrode. This then combines with the appropriate model of the reactor operation, with some assumed 'mixing/hydrodynamic' characteristics. This is constituted in a set of material balances.
- A condition relating to reactor operation. This may be constant electrode potential, cell voltage or current control.
- A charge balance for the system.

The overall model of the reactor system is constituted as an initial value problem and numerical solution can be achieved by several methods for time dependent, nonlinear, differential equations. Generally, the solution is achieved by first solving the model of the reaction in the diffusion layer to give appropriate (species) flux terms into the bulk of the reactor. In the following example this is done analytically. With the input values of the flux terms into the reactor material balance the model is solved numerically by integration over incremental time intervals, until a history of the reactor performance is obtained.

As an example of the way in which electrochemical/chemical reaction schemes can be modelled the derivation of the equations for the following ECE sequence is considered:

$$A + n_1 e^- \xrightarrow{k_{f1}} B \qquad (1a)$$

$$B \xrightarrow{k_{f2}} C \qquad (1b)$$

$$C + n_3 e^- \xrightarrow{k_{f3}} D \qquad (1c)$$

In the ECE scheme shown, an initial electroactive reactant A undergoes electrochemical reaction at the electrode surface to form B. B is not electroactive, but may react chemically to form another electroactive species C. C may then react electrochemically to the final species D. The desired product from such a reaction sequence may be the final product D, or may be one of the intermediate species, B or C. Modelling can reveal the optimum reaction conditions for production of the required species.

In the formulation of the equations for this model, it is assumed that neither the reactions nor mass

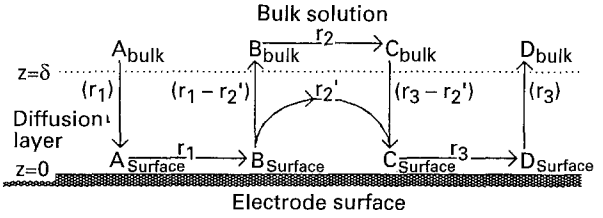

Fig. 1. Schematic reaction model of the ECE scheme.

transport are rate limiting. Thus all of these steps must be included in the model.

The rates of the heterogeneous electrochemical reactions at the electrode surface are r_1 and r_3 for the reactions represented in Equations 1(a) and 1(c), respectively. The chemical reaction rate in the bulk of the electrolyte is r_2, but in some cases it may be important to model separately the chemical reaction within the diffusion layer. r_2' is the overall rate of reaction of species B within the reaction layer. It is helpful when using this approach to represent the reaction rates schematically as illustrated in Fig. 1. The Figure shows the sequence of mass transport and reaction steps and includes the electrochemical and chemical reaction rates.

In this example, it is assumed that all reactions are first order and irreversible, though the method is not limited to such cases. The four reaction rates are expressed by the following equations:

$$r_1 = a_e k_{f1} C_A^s \tag{2}$$

$$r_2 = k_2 C_B^b \tag{3}$$

$$r_3 = a_e k_{f3} C_C^s \tag{4}$$

$$r_2 = a_e k_2 \int_0^\delta C_B^z \, dz \tag{5}$$

3. Reduction to bulk concentrations

To eliminate the surface concentration terms from Equations 2 and 4 and the diffusion layer concentration from Equation 5, it is necessary to use a steady state approximation for the concentrations of species within the diffusion layer. The mass transport rates across the interface between the diffusion layer and the bulk of the electrolyte can be expressed in terms of the reaction rates.

The rate of mass transport of A to the electrode is r_1 and can be written:

$$r_1 = a_e k_{LA}(C_A^b - C_A^s) \tag{6}$$

where k_{LA} is the mass transfer coefficient.

The reaction rate r_1, in terms of the bulk concentration is obtained from Equations 2 and 6 as

$$r_1 = a_e \left(\frac{k_{f1} k_{LA}}{k_{f1} + k_{LA}}\right) C_A^b \tag{7}$$

For species B, the concentration profile is nonlinear if there is appreciable reaction within the diffusion layer. Using the steady state assumption that there is no accumulation of B within this layer, then an instantaneous molar balance over a thickness Δz gives the variation of concentration of intermediate B with distance from the electrode

$$\frac{d^2 C_B^z}{dz^2} - \frac{k_2}{D_B} C_B^z = 0 \tag{8}$$

Boundary conditions at the electrode surface and the edge of the diffusion layer are:

(a) At the electrode surface, assuming that no chemical reaction occurs in the plane of the electrode:

$$r_1 = a_e (N_B)_{z=0} = -a_e D_B \left(\frac{dC_B}{dz}\right)_{z=0} \tag{9}$$

(b) At the interface between the diffusion layer and the bulk of the electrode:

$$(C_B^z)_{z=\delta} = C_B^b \tag{10}$$

Integration of Equation (8) then gives the concentration profile of intermediate B within the diffusion layer:

$$C_B^z = \frac{C_B^b \cosh\left(\frac{Haz}{\delta}\right) + \frac{r_1}{a_e Hak_{LB}} \sinh\left(Ha\left[1 - \frac{z}{\delta}\right]\right)}{\cosh(Ha)} \tag{11}$$

where $Ha = \sqrt{(k_2 D / k_L B)}$.

Substituting this result into Equation 5 gives the total chemical reaction rate within the diffusion layer:

$$r_2' = a_e k_{LB} Ha \tanh\{Ha\} c_B^b + r_1(1 - \operatorname{sech}\{Ha\}) \tag{12}$$

Species C is treated in a similar way to species B and the concentration profile of intermediate C within the diffusion layer is

$$C_C^z = C_C^b + \frac{D_B}{D_C}(C_B^b - C_B^z) - \left[1 - \frac{z}{\delta}\right]\left[\frac{k_{f3}}{k_{f3} + k_{LC}}\right] \times \left[C_C^b - \frac{r_1}{a_e k_{f3}} - \frac{r_1 \tanh\{Ha\}}{a_e Hak_{LC}} + \frac{D_B}{D_C}(1 - \operatorname{sech}\{Ha\}) C_B^b\right] \tag{13}$$

Substituting this result with $z = 0$ into Equation 4 gives the rate of the second electrochemical reaction:

$$r_3 = \left[\frac{k_{f3}}{k_{f3} + k_{LC}}\right] r_1 + a_e \left[\frac{k_{f3} k_{LC}}{k_{f3} + k_{LC}}\right] \times \left[C_C^b - \frac{r_1 \tanh(Ha)}{a_e Hak_{LC}} + \frac{D_B}{D_C}(1 - \operatorname{sech}(Ha)) C_B^b\right] \tag{14}$$

The only concentration terms in these equations are those in the bulk electrolyte.

4. Electrochemical reactor models

The integration of the reaction model derived in Section 3, with material balances and appropriate equations representing the mode of reactor control, is now considered.

4.1. *Batch reactor models*

In this Section, the equations for the case of a potentiostatic batch (or plug flow) reactor are considered.

The concentrations of species in the well mixed bulk of the electrolyte are altered only by the effects of reaction, there being no input or output streams to the volume under consideration. From Fig. 1 the rates of change of bulk concentration for each species are

$$\frac{dC_A^b}{dt} = -r_1 \tag{15}$$

$$\frac{dC_B^b}{dt} = r_1 - r_2' - r_2 \tag{16}$$

$$\frac{dC_C^b}{dt} = r_2 - r_3 + r_2' \tag{17}$$

$$\frac{dC_D^b}{dt} = r_3 \tag{18}$$

Equations 15 to 18 were programmed using ACSL [16] which is a Fortran based language written specifically for non linear, differential equation solution. The numerical integrator is based on an Adam's Moulton routine for stiff differential equation. Further details of the procedures and programmes can be found in [17].

Some typical results from the simultation are presented in Figs 2 and 3. Dimensionless concentrations, ie. C_A/C_{A0} etc., and normalized current density, i/i_0, are plotted against a dimensionless time-dependent parameter, T ($= a_e k_{fl} t$), or against conversion of initial reactant, X_A. Figures 2 and 3 illustrate the effect of variations of the ratios $k_2/(a_e/k_{fl})$ and k_L/k_{fl}, respectively.

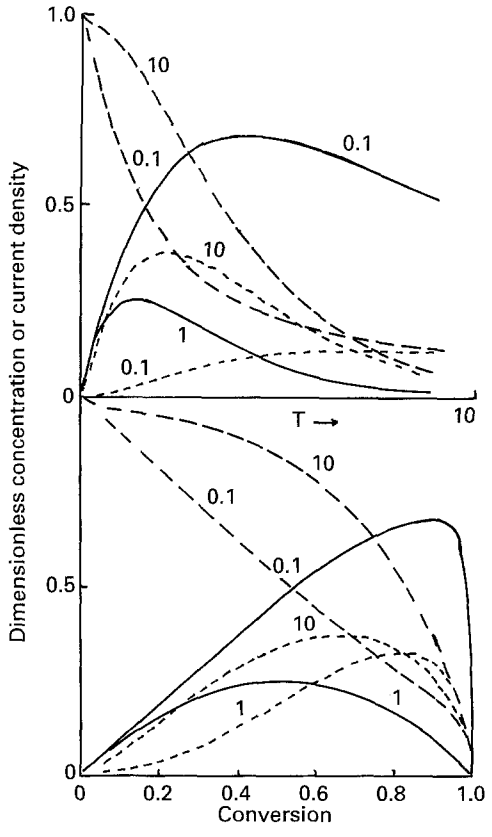

Fig. 2. Variation of dimensionless concentration distribution and dimensionless current density with time and conversion for the ECE scheme during potentiostatic operation. $a_e = 10\,m^{-1}$, $C_{A0} = 100\,kmol\,m^{-3}$, $D = 10^{-9}\,m^2\,s^{-1}$, $k_{fl} = 10^{-5}\,m\,s^{-1}$, $k_{f3}/k_{fl} = 1$, $k_L/f_{fl} = 1.0$. Values of $k_2/a_e k_{fl}$ shown on figure. Curves: (——) C_B/C_{A0}, (- - - -) C_c/C_{A0}, (– – –) i/i_0.

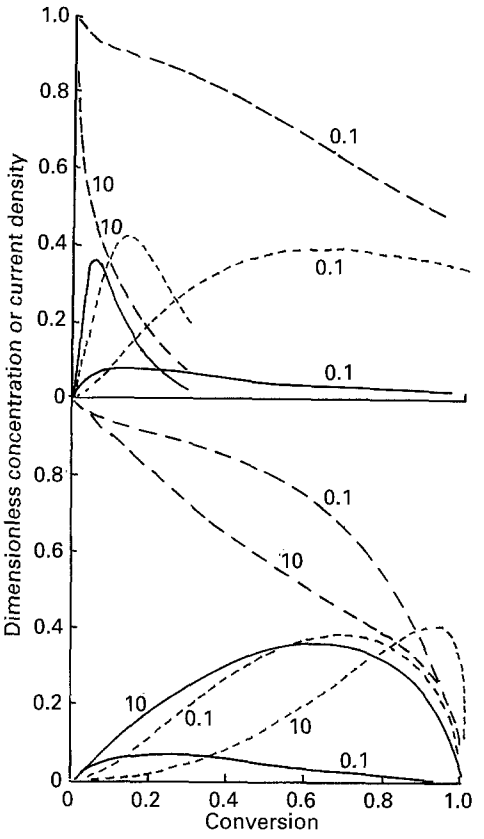

Fig. 3. The effect of mass transport on potentiostatic operation of the ECE scheme. Conditions as Fig. 2. $k_{f3}/k_{fl} = 1$, $k_2/a_e k_{fl} = 1.0$. Values of k_L/k_{fl} shown on Figure. Curves: (——) C_B/C_{A0}, (- - - -) C_c/C_{A0}, (– – –) i/i_0.

The trends perceptible from Fig. 2 are that an increase in the chemical rate constant, k_2, reduces the maximum concentration of B markedly, and increases that of C to a lesser extent. The peak concentrations of both intermediates occur at shorter times (and hence lower conversions) as the ratio $k_2/(a_e/k_{fl})$ is increased. At short times, normalized currents are higher for higher values of $k_2/(a_e/k_{fl})$. At short times, normalized currents are higher for higher values of $k_2/(a_e/k_{fl})$, but later they fall more rapidly so that near the end of the electrolysis, normalized currents are lower at higher values of $k_2/(a_e/k_{fl})$.

Figure 3 illustrates the effect of variations in the mass transfer coefficients k_L. The most marked effect is that on reducing k_L, the rate of the electrochemical steps is slowed due to the lower surface concentrations of A and C, and so the concentration–time characteristics are very different for the two cases shown. Other effects are more readily perceived from the concentration–conversion curves. Reducing k_L increases the diffusion layer thickness, and thus increases the effect of chemical reaction within the diffusion layer, particularly in relation to the slower electrochemical steps. The maximum concentration of intermediate

B is significantly reduced by a reduction in the ratio k_L/k_{f1}, and that of C is increased to a lesser extent. The peak concentrations of both intermediates occur at lower conversions as k_L/k_{f1} is reduced, although the reaction times to reach the peak are longer.

4.2. *Model of the ECE reaction for a CSTR and a recycle reactor*

For the continuous stirred tank and recycle reactor models, the reaction rate equations used for the batch or plug flow reactor model are applicable, since these are independent of reactor type. The only equations which are dependent on reactor type are the differential equations obtained from a material balance over the reactor.

4.2.1. CSTR model. For a continuous stirred tank reactor, shown schematically in Fig. 4, of volume V and inlet and outlet flowrates Q, the ratio V/Q is defined as the space–time, τ. If the outlet stream is assumed to have the same composition as the well mixed bulk of the electrolyte, and if the inlet stream concentrations of the species involved in the reaction are C_{A0}, C_{B0}, C_{C0} and C_{D0}; then the rates of change of bulk concentration of each species are

$$\frac{dC_A^b}{dt} = \frac{[C_{A0} - C_A^b]}{\tau} - r_1 \qquad (19)$$

$$\frac{dC_B^b}{dt} = \left[\frac{C_{B0} - C_B^b}{\tau}\right] + r_1 - r_2' - r_2 \qquad (20)$$

$$\frac{dC_C^b}{dt} = \left[\frac{C_{C0} - C_C^b}{\tau}\right] + r_2 - r_3 + r_2' \qquad (21)$$

$$\frac{dC_D^b}{dt} = \frac{[C_{D0} - C_D^b]}{\tau} + r_3 \qquad (22)$$

Figure 5 illustrates typical dimensionless concentration–time behaviour as the reaction progresses from initial conditions to steady state operation. The space–time of this reactor is 4.4×10^4 s, which is about half the time required for the reactor to reach steady state. The concentrations of both intermediates pass through a maximum before steady state operation is reached, and this may be important in

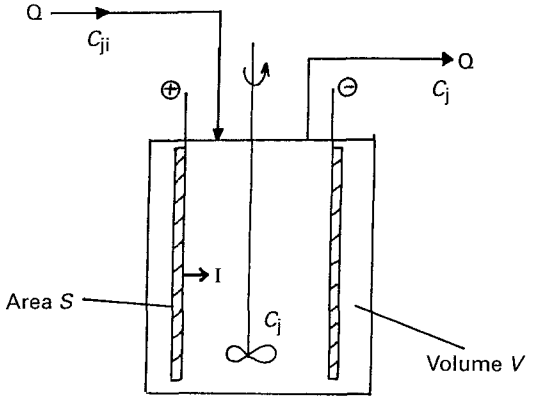

Fig. 4. Schematic model of the continuous stirred tank reactor.

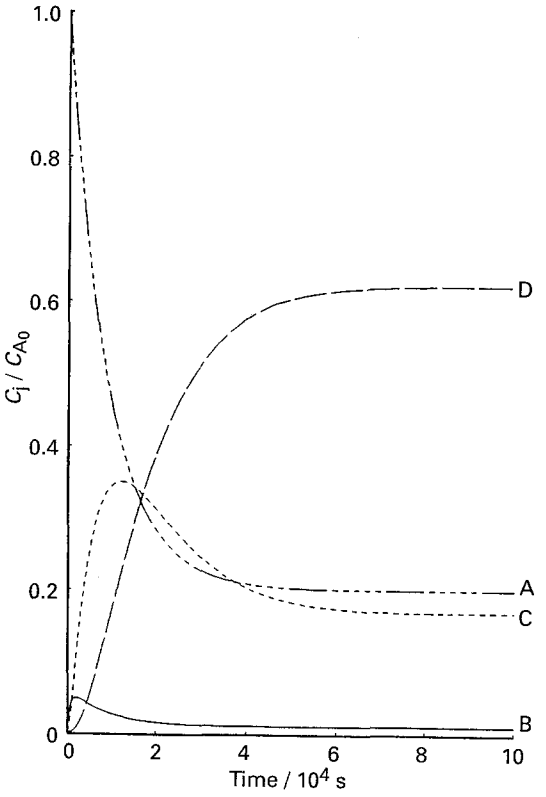

Fig. 5. Dynamic simulation of a continuous stirred tank reactor. $k_2/a_e k_{f1} = 1.5$, $k_{f3}/k_{f1} = 0.5$, $k_L/k_{f1} = 0.1$. Curves: (——) B, (- - - -) C, (– – –) D.

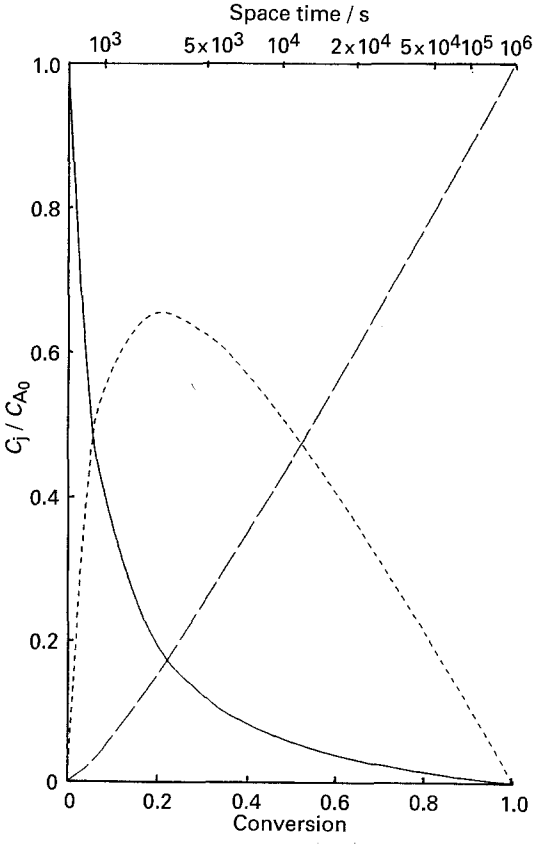

Fig. 6. Variation of steady state product yield for CSTR operation. Conditions as in Fig. 5. Curves: (——) intermediate B, (- - - -) intermediate C, (– – –) product D.

the design of downstream processes. The maximum concentrations in this case are over four times the steady state concentration for B and over twice the steady state value for C.

Figure 6 shows typical variations in steady state product yields with conversion for a CSTR. The figure also shows the equivalent values of space time to achieve these values of yields. Low space–times give low conversions and produce mostly the intermediates B and C. Longer space–times increase both the conversion and the yield of the final product D.

4.2.2. Recycle reactor model. A recycle reactor shown schematically in Fig. 7, is characterized by the recycle ratio, R, the space–time, τ, and the nature of the recycle loop. The recycle ratio is defined as the ratio of the volumetric flowrate recycled to the reactor inlet to the flowrate leaving the system. The space–time is the volume of the electrochemical reactor divided by the volumetric flowrate leaving the system, and hence is not the same as the residence time per pass of the electrolyte τ^1:

$$\tau = \frac{V}{Q} = (R+1)\tau^1 \tag{23}$$

Subscript 'o' refers to the fresh feed, 'i' to the electrolyte entering the reactor, 'e' to the electrolyte leaving the reactor and 'r' to the electrolyte recycled prior to mixing with the fresh feed.

The relationship between the concentrations C_{Ae} and C_{Ar} etc. depends on the nature of the recycle loop. Heterogeneous electrochemical reactions will cease when the electrolyte leaves the reactor and hence

$$C_{Ar} = C_{Ae} \tag{24a}$$

and

$$C_{Dr} = C_{De} \tag{24b}$$

If the recycle is assumed to be instantaneous, then no chemical reaction will occur, and

$$C_{Br} = C_{Be} \tag{25a}$$

and

$$C_{Cr} = C_{Ce} \tag{25b}$$

If the recycle loop is assumed to be equivalent to a plug flow reactor with a residence time τ_r, then chemical reaction will consume some B to produce C. For the first order reaction assumed here, the concentration of B is given by

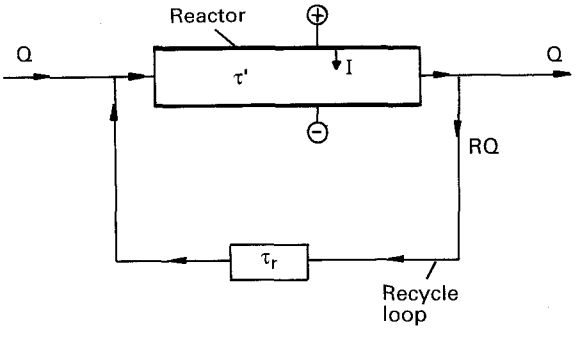

Fig. 7. Schematic diagram of the recycle reactor.

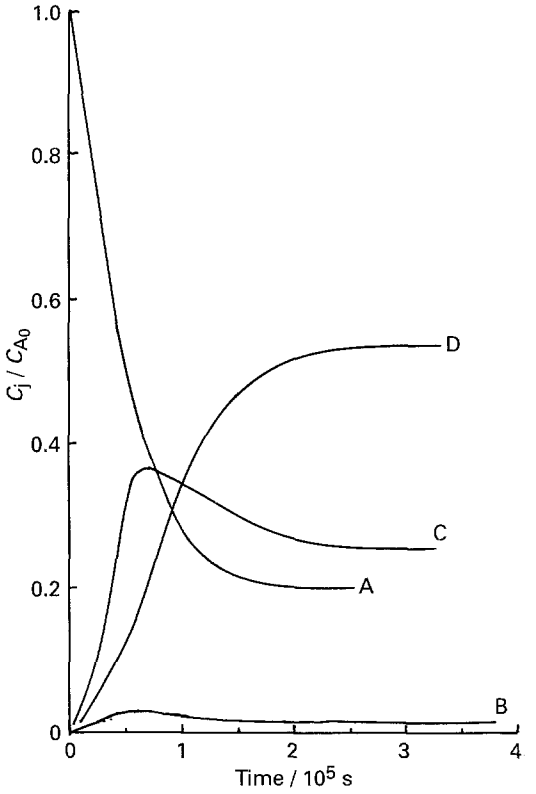

Fig. 8. Dynamic simulation of a recycle reactor with the ECE reaction scheme. Conditions as in Fig. 5.

$$C_{Br} = C_{Be} \exp\{-k_2\tau_r\} \tag{26}$$

and the concentration of C increases by the amount of B which has reacted

$$C_{Cr} = C_{Ce} + C_{Be} - C_{Br} \tag{27}$$

If the recycle loop is assumed to be a well mixed reservoir, equivalent to a CSTR with a residence time of τ_r then

$$C_{Br} = \frac{C_{Be}}{1 + k_2\tau_r} \tag{28}$$

and C_{Cr} is again given by Equation 27.

Once the concentrations, C_{jr}, at the end of the recycle loop have been evaluated, the new inlet stream to the electrochemical reactor is given by the mixture of this stream with fresh feed. Inlet concentrations are calculated by material balances over the mixing junction, giving equations of the form:

$$C_{ji} = \frac{C_{jo} + RC_{jr}}{R+1} \tag{29}$$

A dynamic model of a recycle reactor will be similar to the batch or plug flow model.

Figure 8 illustrates the variation of outlet concentrations with time for a reactor with a recycle ratio of 2. The recycle loop is taken to be equivalent to a tubular plug flow reactor with a residence time equal to 50% of the space–time of the electrochemical reactor element, τ. The overall conversion at steady state is 80%, which is the same as that for the CSTR of Fig. 5, although the conversion per pass in the electrochemical reactor is 57.1%. At least five passes through the reactor are required before steady state is

Table 1. Comparison of different reactors giving 80% conversion

Reactor type	*Recycle loop*	*Space–time*/s	*Yields*/%		
			B	*C*	*D*
CSTR	–	44000	1.48	21.11	77.41
Recycle, $R = 10$	PFR, $\tau_r = 18045$	36085	1.59	24.33	74.08
Recycle, $R = 2$	PFR, $\tau_r = 13710$	27415	1.60	31.62	66.78
Recycle, $R = 0.5$	PFR, $\tau_r = 10510$	21020	1.60	38.52	59.88
Batch or PFR	–	17695	1.60	43.64	54.76

approached. As in the case of the CSTR, the concentrations of both intermediates pass through a maximum before steady state operation is reached, though the ratios of maximum to steady state concentrations are lower in the recycle reactor than in the CSTR. The variations in steady state product yields with conversion for a recycle reactor are very similar to those for a CSTR (see Fig. 6), the most marked difference being that yields of intermediate C are higher and of D lower for a recycle reactor, and space–times to achieve a given conversion are shorter for recycle reactors than for a CSTR.

Table 1 compares results from a number of different ideal reactors which all give a steady state conversion of 80% for the same reaction conditions. The reactors vary in size and in the product distributions obtained. A recycle reactor with a recycle ratio of infinity would represent ideal mixed flow, i.e. a CSTR, and a recycle reactor with $R = 0$ a plug flow reactor. Recycle reactors with intermediate values of R then represent intermediate degrees of backmixing, with behaviour approaching that of a CSTR when R is high and that of a plug flow reactor when R is low. This trend can be seen in Table 1. Plug flow reactors give the lowest volume requirement to achieve a given conversion, but increasing degrees of backmixing favour production of the final species D over that of the intermediate C.

4.3. *Galvanostatic operation*

Operation of reactors under potentiostatic control usually results in a reduction of current density, and hence production rates, as conversion rises, as can be seen in Figs 2 and 3. Higher overall production rates may be achieved by operating at a constant current density, although this change can also affect product distributions. Therefore, it is desirable to be able to model galvanostatic operation within the numerical modelling approach of this paper.

This is achieved by replacing the electrochemical rate constants with expressions which include the effect of potential, for example

$$k_{fi} = [k_{fi}^1]_0 \exp[-\beta_i(E - E_e)] = [k_{fi}]_0 \exp[-\beta_i E] \tag{30}$$

where $\beta_i = \alpha n_i F/RT = -2.3/b$ is related to the Tafel slope b.

The potential E is measured relative to the potential at the beginning of a galvanostatic run. Thus $(k_{fi})_0$ is the value of k_{fi} at the start of the electrolysis when $E = 0$. Potentials calculated at other times are expressed relative to the starting potential.

To incorporate galvanostatic operation into a simulation program, two subroutines are added to calculate new values of potential for each integration time increment from the current balance. This uses an interatine routine based on the modified *regula falsi* algorithm, which will always converge provided that the i_T/E curve is continuous and monotonic and the reaction is not mass transfer limited. Successive iterations locate new potentials giving a total current sufficiently close to the initial value.

The program checks whether the limiting current, which falls as the concentrations of electroactive species falls, is close to the value of i_0. If i_0/i_L exceeds a specified value, say 0.99, the reaction is deemed mass

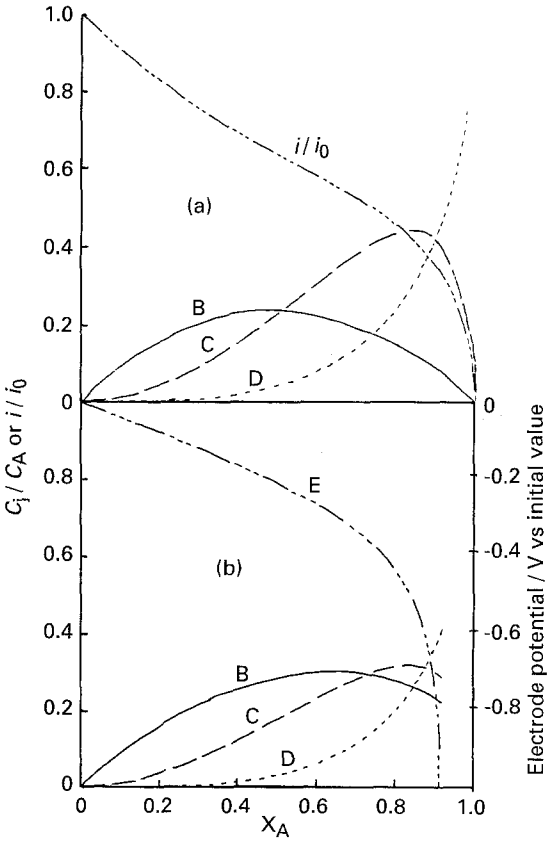

Fig. 9. Comparison of galvanostatic operation with potentiostatic operation for the ECE reaction scheme. (a) Potentiostatic operation, and (b) galvanostatic operation.

transfer limited and galvanostatic operation can no longer be maintained. The limiting current is found by putting $k_{fi} \gg k_L$ into the reaction rate equations.

For the ECE reaction sequence, the limiting current density is given by

$$i_L = Fk_L\left[\left(n_1 + n_3\left\langle 1 - \frac{\tanh(Ha)}{Ha}\right\rangle\right)C_A^b + n_3(C_c^b + \langle 1 - \operatorname{sech}(Ha)\rangle C_B^b)\right] \quad (31)$$

Figure 9 illustrates the differences in the concentration–conversion behaviour of an ECE reaction in a batch reactor under potentiostatic and galvanostatic control. Under galvanostatic conditions, the reaction does not proceed to complete conversion, since mass transport limitations prevent the maintenance of constant current when the concentrations of electroactive species fall to low levels. For the conditions of Fig. 9, the reaction becomes limited by mass transport when a conversion of approximately 90% has been achieved.

Galvanostatic operation causes an increase in electrochemical rate constants as the reaction proceeds, whilst the chemical rate constants do not change. Thus it is expected that operation at constant current favours the production of intermediate B at the expense of C when compared to potentiostatic operation. This behaviour is seen in Fig. 9. Also shown on the figure are the variations of i/i_0 (for potentiostatic operation) and electrode potential E (for galvanostatic operation).

4.4. *Plug flow reactor models with constant cell voltage*

The plug flow reactor models described earlier can only be considered approximations to industrial electrolytic reactors. This is because the models have assumed that either the electrode overpotential or the current density remains constant along the whole length of the reactor. These assumptions are invalid unless the conversion in the reactor is low, or unless the reactor is divided into many short, independently controlled electrode sections such that the conversion in any one section is low. If a more accurate simulation of plug flow is required, then a technique similar to that described for the simulation of galvanostatic operation can be used. The method by which this is implemented is outlined below.

The true condition of each independent section of a plug flow reactor is that E_C, the voltage between the two electrodes, is constant (assuming a constant electrode phase potential).

$$E_c - [(E_e)_{anode} - (E_e)_{cathode} = |\eta_a| + |\eta_c| + 1000 i_T \, d\kappa = \text{constant} \quad (32)$$

This equation requires some consideration to be given to the reactions at the counter electrode. If, for example, the reactions of interest occur at the cathode and in an aqueous solution, then a common accompanying anode reaction is the evolution of oxygen. If the species present are not easily oxidized at the anode, then oxygen evolution is the dominant anode reaction and the partial current density for oxygen evolution, i_{02}, is approximately equal to the total current density, i_T. Substituting a Tafel type equation for η_a, Equation 32 becomes:

$$a_{0_2} + b_{0_2}\log_{10}(i_T) + |E_{cathode} - (E_e)_{cathode}| + 1000 i_T \, d\kappa = \text{constant} \quad (33)$$

or, with the convention that $E_{cathode} = 0$ at the beginning of the electrolysis:

$$|E_{cathode}| + \frac{\log_e T}{\beta_{0_2}} + 1000 i_T \, d\kappa = \frac{\log_e o}{\beta_{0_2}} + 1000 i_0 \, d\kappa \quad (34)$$

where $\beta_{0_2} = -(1 - \alpha_{0_2})n_{0_2}F/RT$.

The condition of Equation 34 can replace the condition of constant current in the iteration subroutine used for galvanostatic operation and the resulting ACSL program will satisfactorily model plug flow reactors. Such modelling procedures can readily be extended to accommodate the variation of electrolyte conductivity in the direction of electrolyte flow due to the generation of gas bubbles.

Figure 10 shows the concentration–conversion curves for an ECE reaction in a plug flow reactor, illustrating the differences between the approximate model of Section 2 and the more exact, constant cell voltage model of this section. At low conversions, the results from the two models coincide. As conversion increases, the exact model predicts a less

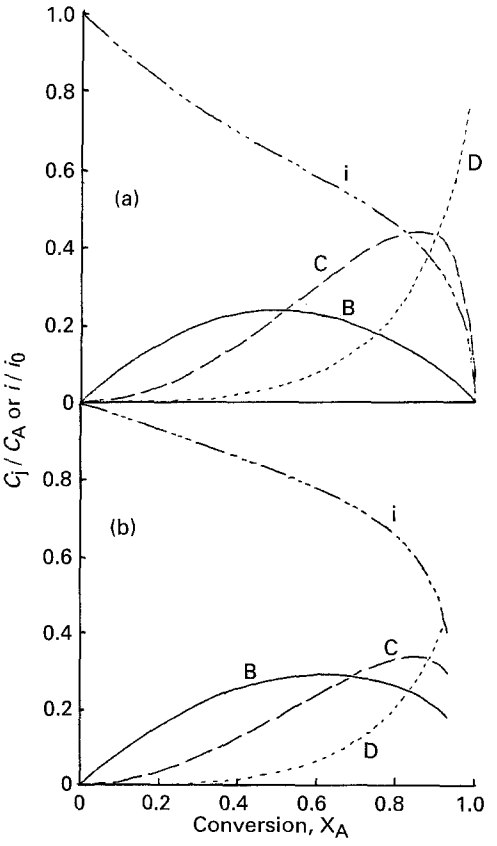

Fig. 10. Comparison of product distribution during constant voltage operation and potentiostatic operation. (a) Potentiostatic, (b) constant voltage. $\beta_{0_2} = 39\,V^{-1}$, $d\kappa = 2 \times 10^{-2}\,\Omega^{-1}$.

rapid decrease in current density than does the approximate model, and the exact model also predicts an increase in cathode overpotential with increasing conversion. Electrochemical rate constants thus increase to a greater extent in the exact model compared to the approximate model, so that production of C is reduced by operation at constant cell voltage. This behaviour can be seen in the Figure at conversions greater than 50%.

4.5. *Solvent decomposition*

The occurrence of a parasitic side reaction such as decomposition of the electrolyte solvent is common in industrial operation and results in an additional loss of current efficiency. The inclusion of such an effect within the modelling approach is achieved by the addition of further reaction rate equations describing the side reaction. In the case of solvent decomposition, when there is a large excess of the solvent, the concentration changes arising from these reactions are negligible, and the solvent decomposition rate during a run can be taken to be dependent only on potential. The dimensionless parameter used to characterise the solvent decomposition rate is $(r_h)_0/(a_e/C_{A0}k_{f1})$, where $(r_h)_0$ is the rate of solvent decomposition at the beginning of the electrolysis, and $a_eC_{A0}k_{f1}$ is the initial rate of the first electrochemical reaction in the absence of mass transfer limitations.

The effects of solvent decomposition on product distributions are most marked in galvanostatic operation, since the additional reaction significantly alters the potential–time behaviour of the working electrode. The rate of solvent decomposition during a galvanostatic run is conveniently given by

$$r_h = (r_h)_0 \exp[-\beta_h E] \qquad (35)$$

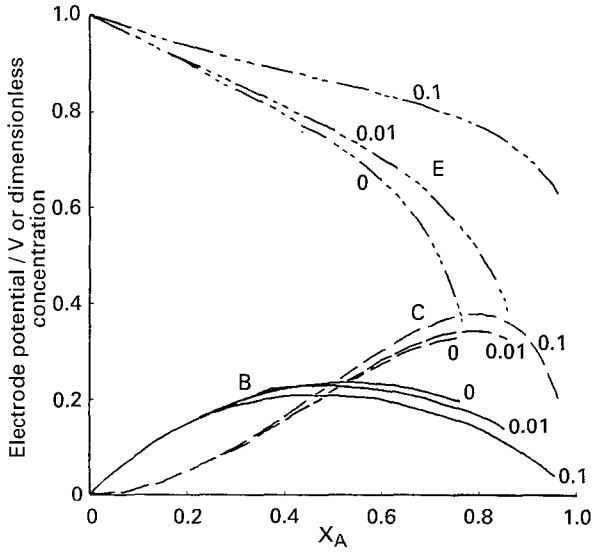

Fig. 11. The influence of solvent decomposition on galvanostatic operation of a batch reactor. (Values of the dimensionless reaction rate for solvent decomposition $(r_h)_0/a_eC_{A0}K_{f1}$, shown on figure) Curves: (——) C_B/C_{A0}, (– – –) C_C/C_{A0}, (– · · –) electrode potential.

and this reaction rate is included in the expression for the total current.

Fig. 11 illustrates the effects of different degrees of solvent decomposition on the product distributions obtained from the galvanostatic operation of a batch reactor. Since there is assumed to be no change in the concentrations of electroactive species involved in the solvent decomposition reaction, the potential required to maintain constant current is less cathodic, the greater the degree of solvent decomposition. This, in turn, reduces the rate of increase of electrochemical rate constants during the reaction. As noted in Section 4.4 the increase in electrochemical rate constants favours production of intermediate B over C. Thus greater degrees of solvent decomposition will reverse this behaviour and favour the production of intermediate C. These trends are shown in Fig. 11. A further effect of the occurrence of solvent decomposition, also shown in the figure, is to delay the onset of mass transfer limitation.

5. Conclusions

A modelling approach has been described which satisfies the requirements of operation of many electrochemical reactors. For the example of an ECE reaction scheme, the application of the method has been demonstrated and some typical results presented. To generalize the approach to other reaction schemes, the overall procedures adopted can be followed.

From a limited amount of kinetic and physical data, predictions of the variations in concentration and potential or current are made for several different reactor types during galvanostatic or potentiostatic operation, with the effects of solvent decomposition taken into account. Alternatively, experimentally derived concentration–time behaviour can be used to determine approximate kinetic and physical data, by comparison with simulated reaction model results.

Such simulations can be used to fine tune experimental derived rate data for the overall objective of improved process modelling.

References

[1] S. W. Feldberg, *in* Electroanalytical Chemistry, Vol. III, (edited by A. J. Bard) Marcel Dekker, New York (1969).
[2] I. Ruzic and S. W. Feldberg, *J. Electroanal. Chem.* **50** (1974) 153.
[3] D. N. Bennion, *AIChE Symposium Series*, No 229, **79** (1983) 25.
[4] R. Alkire and A. A. Mirarefi, *J. Electrochem. Soc.*, **120** (1973) 1507.
[5] *Idem, ibid.* **124** (1977) 1043.
[6] *Idem, ibid.* **124** (1977) 1214.
[7] R. Alkire and R. Gould, *J. Electrochem.* **123** (1976) 1842.
[8] R. E. White, S. E. Lorimer and R. Darby, *J. Electrochem. Soc.* **130** (1983) 1123.
[9] R. E. White, M. Bain and M. Raible, *ibid.* **130** (1983) 1037.
[10] T. V. Nguyen, C. W. Walton, R. White and J. van Zee, *J. Electrochem. Soc.* **133** (1986) 81.

[11] R. C. Alkire and J. D. Lisius, *J. Electrochem. Soc.* **132** (1985) 1879.
[12] J. D. Lisius, MS thesis, University of Illinois, Urbana, IL (1982).
[13] E. K. Yung and R. C. Alkire, *J. Electrochem. Soc.* **132** (1985) 2341.
[14] J. C. Yu, M. M. Baizer and K. Nobe, *ibid.* **135** (1988) 1392.
[15] C. Oloman and P. Reilly, *ibid.* **134** (1987) 859.
[16] 'Advanced Continuous Simulation Language – User guide/ Reference Manual', 3rd edn, Mitchell and Gauthier, Concord, MA (1981) p. iii.
[17] A. N. Haines, PhD thesis, Teesside Polytechnic, UK (1988).